

Tunable interlayer magnetism and band topology in van der Waals heterostructures of MnBi₂Te₄-family materials

Zhe Li^{1,2,†}, Jiaheng Li^{1,2,†}, Ke He^{1,2,3,*}, Xiangang Wan^{4,5}, Wenhui Duan^{1,2,3,6}, and Yong Xu^{1,2,7,*}

¹State Key Laboratory of Low-Dimensional Quantum Physics, Department of Physics, Tsinghua University, Beijing 100084, China

²Frontier Science Center for Quantum Information, Beijing 100084, China

³Beijing Institute of Quantum Information Science, Beijing 100193, China

⁴National Laboratory of Solid State Microstructures and School of Physics, Nanjing University, Nanjing 210093, China

⁵Collaborative Innovation Center of Advanced Microstructures, Nanjing 210093, China

⁶Institute for Advanced Study, Tsinghua University, Beijing 100084, China

⁷RIKEN Center for Emergent Matter Science (CEMS), Wako, Saitama 351-0198, Japan

[†]These authors contributed equally to this work.

*Correspondence to: yongxu@mail.tsinghua.edu.cn (Y. X.); kehe@tsinghua.edu.cn (K. H.).

Manipulating the interlayer magnetic coupling in van der Waals magnetic materials and heterostructures is the key to tailoring their magnetic and electronic properties for various electronic applications and fundamental studies in condensed matter physics. By utilizing the MnBi₂Te₄-family compounds and their heterostructures as a model system, we systematically studied the dependence of the sign and strength of interlayer magnetic coupling on constituent elements by using first-principles calculations. It was found that the coupling is a long-range superexchange interaction mediated by the chains of *p* orbitals between the magnetic atoms of neighboring septuple-layers. The interlayer exchange is always antiferromagnetic in the pure compounds, but can be tuned to ferromagnetic in

some combinations of heterostructures, dictated by d orbital occupations. Strong interlayer magnetic coupling can be realized if the medial p electrons are delocalized and the d bands of magnetic atoms are near the Fermi level. The knowledge on the interlayer coupling mechanism enables us to engineer magnetic and topological properties of MnBi_2Te_4 -family materials as well as many other insulating van der Waals magnetic materials and heterostructures.

Van der Waals (vdW) layered magnets have attracted intensive attentions in the recent years (1-6). Benefitting from the weak vdW interlayer bonding, these materials can be easily exfoliated into ultrathin flakes and flexibly recombined into various heterostructures with novel material properties. Many layered magnetic materials have been found, including $\text{Cr}_2\text{Ge}_2\text{Te}_6$, CrI_3 , $\text{Fe}_2\text{Ge}_2\text{Te}_6$, FePS_3 , VSe_2 , MnSe_2 (7-22), and the MnBi_2Te_4 -family compounds (23-34), which provide new chances for developing electronics, spintronics, optoelectronics, and topological physics (4-6, 23-39). A key ingredient to designing and engineering vdW magnetic materials and heterostructures for various purposes is to manipulate the interlayer magnetic coupling (IMC), i.e., the magnetic coupling across the vdW gap. The sign and strength of IMC have been found to vary significantly in different vdW magnets, and a comprehensive understanding on the underlying mechanism is still lacking.

The MnBi_2Te_4 -family compounds as vdW layered intrinsic magnetic topological materials are particularly interesting for the rich magnetic topological phases they host, including the antiferromagnetic (AFM) topological insulator (TI) (23-34, 39) and the magnetic Weyl semimetal (WSM) (23-26, 34) in the 3D bulk, as well as the quantum anomalous Hall (QAH) insulator (23-29, 33, 34) and axion insulator (23-28) in their 2D films. Quantized transports have been observed in MnBi_2Te_4 thin flakes at relatively high temperatures ($>1\text{K}$) (28, 29, 33). Crystallized in a rhombohedral layered structure, bulk tetradymite-type MnBi_2Te_4 is composed of vdW-bonded septuple-layers (SLs). Each SL is consisted of seven atomic layers, of triangular lattice with ABC-stacking (23-25) in the sequence of Te/Bi/Te/Mn/Te/Bi/Te (Fig. 1(a)). The intralayer magnetic

coupling is ferromagnetic (FM) with an out-of-plane easy magnetic axis, while the IMC is AFM. Thus the MnBi_2Te_4 bulk has an A-type AFM ground state.

The MnBi_2Te_4 -family materials provide an excellent platform to explore the IMC mechanism of vdW magnets. Firstly, the ternary-compound family includes many candidate materials constituted by different combinations of nonmagnetic and magnetic elements (23), which enables a systematic study on the element-dependence of IMC. Secondly, the relatively long distance between neighboring magnetic atomic layers locks the way of bonds forming and forbids many kinds of electron hopping channels (see a more detailed analysis in Supplemental Material), simplifying the discussions on the IMC mechanism. Besides, since the topological properties of MnBi_2Te_4 -family materials depend critically on the interlayer magnetic state (23-25, 28, 33, 34), the knowledge on the IMC mechanism can be directly used to engineer the magnetic topological quantum states and effects (35-39).

In this *Letter*, we systematically studied the constituent-element-dependence of the IMC of MnBi_2Te_3 -family materials and heterostructures by first-principles calculations. Our results reveal that the IMC is dominated by the long-distance superexchange mechanisms mediated by the p orbitals of non-magnetic atoms. Remarkably, both the sign and strength of IMC can be significantly manipulated by choosing different magnetic elements with different numbers of d electrons and nonmagnetic elements of different electronegativities. This provides us guidelines to understand, design, and engineer the magnetic and topological properties not only for this material family but also for layered magnetic insulators in general.

First-principles calculations were performed in the framework of density functional theory (DFT) using the Vienna *ab initio* simulation package (VASP) (40). The Perdew-Burke-Ernzerhof (PBE) type exchange-correlation functional in the generalized gradient approximation (GGA) (41) was adopted. The localized $3d$ -states of V, Cr, Mn, Fe, Ni and $4f$ -states of Eu were treated by employing the PBE+ U approach ($U = 3.0, 4.0, 4.0, 4.0, 4.0, 5.0$, respectively). The U values have been tested and used by previous works (7, 11, 19-25, 34). Band structures for thin films and bulks were computed by the PBE+ U method and the modified Becke-Johnson (mBJ) functional

(42), respectively. VdW corrections were included by the DFT-D3 method (43). All the crystal structures were fully relaxed. The magnetic ground state and exchange energies for each material were determined by computing energy differences between different magnetic configurations. Topological surface states or edge states were calculated by using WannierTools package based on maximally localized Wannier functions (44). More calculation details are described in the Supplemental Material.

According to the superexchange theory (45, 46), the exchange coupling between two magnetic atoms emerges when an indirect electron hopping between d (or f) orbitals of magnetic elements is mediated by the connecting p orbitals. In the MnBi_2Te_4 -family compounds, magnetic atoms are bonded with six chalcogen atoms in a slightly distorted octahedral geometry, where the d orbitals of each spin state are roughly split to triply degenerate t_{2g} states and doubly degenerate e_g states. Generally, there exist three kinds of hopping channels in the system, including e_g - p - e_g , e_g - p - t_{2g} and t_{2g} - p - t_{2g} , as illustrated in Fig. 1(c). Here σ bonds are formed between e_g and p orbitals, whose strength is much stronger than that of π bonds formed between t_{2g} and p orbitals. Therefore, the e_g - p - e_g hopping channels, if existing, play a dominant role in determining the sign and strength of IMC.

We first analyze the IMC of MnBi_2Te_4 . For the Mn ions, their $3d$ orbitals of one spin (spin-up) channel are fully occupied, and the other spin channel is empty. While the interlayer electron hopping between d orbitals of neighboring Mn atoms is prohibited in the FM configuration, it gets allowed in the AFM configuration (Fig. 1(d)). Therefore, the IMC of MnBi_2Te_4 is AFM, giving an A-type AFM ground state as learned from previous theoretical and experimental works (23-28, 30-32). Further analyses on other MnBi_2Te_4 -family compounds indicate that their IMC is always AFM, independent of constituent elements, as confirmed by our first-principles calculations. This seems to be a disadvantage for research and applications, since sometimes a FM IMC is desired, for instance, for obtaining a non-zero net magnetism and for realizing the QAH effect.

In contrast to pure compounds, vdW heterostructures of XBi_2Te_4 ($\text{X}=\text{Mn}, \text{V}, \text{Ni}, \text{Eu}$) has been rarely explored, which could open new opportunities to tuning magnetic

and topological properties. In particular, we will show that the IMC can be driven into FM in the vdW heterostructures with different magnetic elements. We take the $\text{MnBi}_2\text{Te}_4\text{-EuBi}_2\text{Te}_4$ (MBT-EBT) combination as an example. The schematic lattice structure of the MBT-EBT bilayer is shown in Fig. 1(b). In EuBi_2Te_4 , the $4f$ orbitals of Eu are far away from the Fermi level (E_F), leaving the $5d$ orbitals close to E_F . These $5d$ orbitals are empty and polarized by magnetic moments of the $4f$ electrons, giving spin-up states lower than spin-down ones (47). Although the $e_g\text{-}p\text{-}e_g$ hopping is allowed in both FM and AFM IMC configurations of $\text{MnBi}_2\text{Te}_4\text{-EuBi}_2\text{Te}_4$, the energy difference between the spin-up e_g orbitals of Mn and Eu atoms is smaller in the former case, making the FM coupling energetically more favorable than the AFM one (Fig. 1(e)). Therefore, the IMC between a MnBi_2Te_4 SL and an EuBi_2Te_4 SL is FM (see a detailed analysis in the Supplemental Material). Applying similar analyses to all $\text{XBi}_2\text{Te}_4\text{-YBi}_2\text{Te}_4$ heterostructures, we find that generally the FM IMC emerges when X has d electrons ≥ 5 while Y has d electrons < 5 . In some complicated cases, such as $\text{MnBi}_2\text{Te}_4\text{-VBi}_2\text{Te}_4$, the FM and AFM IMC are comparable in strength, giving rise to relatively weak IMC.

The IMC mechanism is supported by our first-principles calculations. The energy differences between AFM and FM configurations per unit cell (E_{ex}) of a series of $\text{XBi}_2\text{Te}_4\text{-YBi}_2\text{Te}_4$ bilayers (X, Y = Mn, V, Ni, and Eu) are listed in TABLE 1. It is shown that $\text{MnBi}_2\text{Te}_4\text{-EuBi}_2\text{Te}_4$, $\text{MnBi}_2\text{Te}_4\text{-VBi}_2\text{Te}_4$, $\text{NiBi}_2\text{Te}_4\text{-EuBi}_2\text{Te}_4$, and $\text{NiBi}_2\text{Te}_4\text{-VBi}_2\text{Te}_4$ favor FM IMC, and the other combinations favor AFM IMC. The results can be understood by the superexchange theory as discussed above.

Noticeably, the superexchange coupling in magnetic oxides is supposed to be rather short-ranged (45, 46). Typically, only the cation-anion-cation coupling is considered. But the calculated IMC strength between MnBi_2Te_4 -family materials is not negligible though the magnetic atoms from neighboring SLs are spaced by six layers of non-magnetic atoms together with a vdW gap. Especially, $|E_{\text{ex}}|$ between two NiBi_2Te_4 SLs is as high as 16.5 meV. According to the traditional superexchange theory (45, 46), the IMC strength is mainly dependent on the hopping term between magnetic atoms,

which is determined by the overlapping of the relevant orbitals in real space. In magnetic oxides, the electronegativity difference between oxygen ($\chi = 3.44$) and magnetic metal atoms (mostly $\chi < 2.00$) is so large that the medial p electrons are rather localized around each oxygen ion. In the MnBi_2Te_4 -family materials, the similar electronegativities between cations (Bi) and anions (Te) lead to much more delocalized p electrons, which may facilitate longer-range magnetic coupling.

To verify the argument, we calculated the dependence of $|E_{\text{ex}}|$ on the non-magnetic elements in $\text{Ni(V)}_2(\text{VI})_4$ compounds, where (V)= Bi or Sb, and (VI)=Te, Se, or S. As shown in Fig. 2(a), replacing Te ($\chi = 2.10$) with Se ($\chi = 2.55$) and S ($\chi = 2.58$) significantly reduces $|E_{\text{ex}}|$, from 16.5meV to 3.5meV and 1.1meV, respectively. The underlying reason is that Te $5p$ electrons are more delocalized than Se $4p$ and S $3p$ electrons in this system, and thus easier to hop to neighboring atoms along the p orbital chain. In contrast, $|E_{\text{ex}}|$ drops to nearly zero ($< 0.1\text{meV}$) if artificially replacing Te with O, which is expected by the typical superexchange coupling for such a large interatomic distance. A similar trend is also found in the $\text{NiSb}_2(\text{VI})_4$ compounds. Replacing Bi ($\chi = 2.02$) with Sb ($\chi = 2.05$) in $\text{NiBi}_2(\text{VI})_4$ enhances $|E_{\text{ex}}|$ to as large as 24.7 meV in the NiSb_2Te_4 bilayer. The relationship of $|E_{\text{ex}}|$ and the electronegativity difference ($\Delta\chi$) of constituent elements are plotted for $\text{Ni(V)}_2(\text{VI})_4$ compounds in Fig. 2(b), which shows a clear inverse correlation.

To further confirm this argument, we analyzed element-projection band structures of bulk NiSb_2Te_4 , NiBi_2Te_4 , NiSb_2Se_4 , and NiBi_2Se_4 along the Γ -Z direction (out-of-plane) (Fig. 2(c)). The wider band dispersion along the Γ -Z direction means the more delocalized p or d electrons along out-of-plane direction. Comparing NiSb_2Te_4 with NiBi_2Te_4 , the dispersion of Te bands in the former case is obviously wider than in the latter, facilitated by a closer electronegativity between Sb and Te. More hybridized and coupled with Te $5p$ bands, Sb $5p$ bands are pushed upward by Te $5p$ bands almost above Ni $3d$ bands, with wider band dispersion than that of Bi $6p$ bands. These band features will definitely lead to larger IMC in NiSb_2Te_4 than NiBi_2Te_4 . Comparing NiSb_2Te_4 with NiSb_2Se_4 , however, two factors are needed to be considered. Firstly, Te shares closer electronegativity to Sb than Se, and Sb $5p$ bands are located nearer to Te $5p$ bands than

Se 4*p* bands. The dispersion of Sb 5*p* bands in NiSb₂Te₄ is thus larger than NiSb₂Se₄, indicating more delocalized *p* electrons. Secondly, Te 5*p* orbitals are more extended than Se 4*p* orbitals, leading to stronger overlapping with Ni 3*d* orbitals and with Te 5*p* orbitals of neighboring SLs in real space. Figure 2(d) shows the zoom-in band structures around Ni 3*d* bands. The 3*d* band dispersion of magnetic atoms is directly related to the IMC strength. Clearly, the dispersions of the four compounds give band widths NiSb₂Te₄>NiBi₂Te₄> NiSb₂Se₄>NiBi₂Se₄, exhibiting the same trend of IMC strength. The dependence of $|E_{\text{ex}}|$ on magnetic elements listed in TABLE I can also be understood with similar analyses. The much stronger IMC of NiBi₂Te₄ bilayer than other XBi₂Te₄-YBi₂Te₄ combinations is because the 3*d* bands of Ni is closer to and thus more strongly hybridized with *p* bands than the *d* bands of other magnetic elements.

The understanding on the IMC mechanism of MnBi₂Te₄-family enables us designing and engineering topological states by controlling the IMC. For example, bulk MBT is an AFM TI in its ground state and becomes a magnetic Weyl semimetal when it is changed into the FM configuration by a large external magnetic field (23-25, 27). The magnetic Weyl semimetal possesses only one pair of Weyl points and is expected to show high-Chern-number QAH phases in thin films (33, 48-52). The FM IMC between MBT and EBT suggests that one may obtain an intrinsic ferromagnetic WSM (in no need of applying external magnetic fields) in MBE-EBT heterostructures.

Figure 3(a) displays the calculated bulk band structure of a MBT-EBT superlattice. A band crossing is observed at E_F near the Γ point along the $\Gamma - Z$ direction. Except for the two crossing points (the other point is along opposite direction symmetrically) and a weakly dispersed band connecting them, no electron or hole pocket exist at E_F . Figure 3(b) gives the Fermi surface of the $(k_x - k_z)$ surface states, showing a Fermi arc connecting the two crossing points (i.e. Weyl points). The band and Fermi surface structures indicate that bulk MBT-EBT is a type-I ferromagnetic WSM possessing only one pair of Weyl points (WPs) (53). By checking the motions of the sum of Wannier charge centers (WCCs), the two WPs show opposite chiralities, as theoretically expected (Fig. 3(c)). We checked the evolution of its band structure with the SOC artificially varied from 75% to 110% of the real strength. The dependence of band gap

at the Γ point on the SOC strength is depicted in Fig. 3(d). The band gap closes twice at 92% and 102%, and the band closing points divide the phase diagram into three parts, including a trivial FM insulator phase, a WSM phase, and a FM insulator phase with band inversion. The last one is a phase named as “FMTI”, which is topologically equivalent to Cr- or V-doped $(\text{Bi,Sb})_2\text{Te}_3$ TIs (54, 55). When the time reversal symmetry is recovered above the Curie temperature, it is a typical TI. Below the Curie temperature, its bulk phase becomes topologically trivial with broken time-reversal symmetry, but its thin films are expected to be QAH insulators with $C=1$ (51).

A 2D thin film of a magnetic WSM can show the QAH effect with the Chern number increasing with the film thickness (33, 51, 52). Figure 4(a) shows the evolution of the Chern number and band gap of MBT-EBT thin films with varying film thickness. The film including one MBT-EBT bilayer is a normal insulator with a zero Chern number due to quantum confinement effects. Thicker films containing 2 to 10 MBT-EBT bilayers are QAH insulators with $C=1$, whose band gap reaches a maximum (about tens of meV) in the 3-bilayer film. In a magnetic WSM film, the increment of Chern number (ΔC) with film thickness satisfies (33): $\Delta C \approx \Delta N |k'_W|$, where $|k'_W|$ denotes the ratio of $\Gamma - W$ to $\Gamma - Z$ along $\Gamma - Z$ direction. For bulk MBT-EBT, $|k'_W| = \frac{0.0717}{0.5} \approx \frac{1}{7}$, which is consistent with the calculation result that $C=2$ from 11 to 17 bilayers and $C=3$ above 18 bilayers. The edge states of a 3-bilayer film and a 12-bilayer film are displayed in Fig. 4(b) and Fig. 4(c), respectively. Clearly, they are QAH insulators with $C=1$ and $C=2$, respectively, showing one and two gapless chiral edge modes crossing the bulk gap.

In this material system, a moderate external hydrostatic pressure can lead to a band inversion at the Γ point, resulting in a topological phase transition (51). Figures. 3(e) and 3(f) present the projection band (p-band) results projected by Bi (blue) and Te (red) under ambient pressure and 0.2 GPa hydrostatic pressure, respectively. Under ambient pressure, there is only one band inversion between Bi p_z and Te p_z bands, which leads to a WSM phase. Under 0.2 GPa pressure, two band inversions occur, opening an insulating band gap. The so-called “FMTI” thus emerges (51). Thin films of this phase

above 2 bilayers are all QAH insulator with $C=1$, as confirmed by edge-state results shown for 3 bilayers (Fig. 4(e)) and 12 bilayers (Fig. 4(f)).

The IMC mechanism of MBT-family materials revealed in this work provides us a universal framework for understanding the magnetism of insulating layered magnetic compounds and their heterostructures. Below we summarize several guiding principles for estimating the IMC of insulating layered materials qualitatively or even quantitatively.

First, the rules for analyzing superexchange interactions in ferrites can basically also be applied to estimate the sign and relative magnitude of IMC. Especially, e_g - e_g hopping through p bands usually dominates the magnetic coupling if present. The IMC of many vdW heterostructures such as $\text{XBi}_2\text{Te}_4\text{-CrI}_3$, $\text{XBi}_2\text{Te}_4\text{-Cr}_2\text{Ge}_2\text{Te}_6$, $\text{XBi}_2\text{Te}_4\text{-FePS}_3$ can be estimated by this way (see Supplemental Material). For systems where e_g - e_g is not the dominated exchange coupling channel, more careful analyses are needed because different hopping channels favoring different kinds of magnetic states may compete (7-10, 12-18).

Second, a stronger IMC requires more delocalized medial p electrons which can be realized by similar electronegativities between cations and anions. It's worth mentioning that heavy nonmetallic elements share the similar electronegativities with heavy metallic elements. One can choose materials including heavier elements near the metal-insulator boundary to obtain a stronger IMC.

Third, the IMC can be further enhanced if the d bands of magnetic ions are near E_F , strongly hybridizing with the p bands. So, Ni^{2+} -based FM or AFM insulators, for example, could contribute to a strong IMC with a neighboring layered magnetic material.

These guiding principles enable us designing and engineering the magnetic properties of magnetic vdW materials for different purposes. The various van der Waals heterostructures composed of different layered magnetic materials will make the principles easily tested and widely applied in experiment.

In conclusion, we systematically studied the IMC mechanism of the MnBi_2Te_4 -family compounds and heterostructures. The superexchange coupling is found to dominate the IMC, and the delocalized p electrons contribute to the relatively strong

coupling strength across a long atomic distance. The understanding on the IMC mechanism implicates the principles of manipulating the interlayer magnetic configurations of insulating vdW magnets, which is especially valuable in exploring novel magnetic topological phases and effects in them.

References

1. A. K. Geim, I. V. Grigorieva, Van der Waals heterostructures. *Nature* **499**, 7459 (2013).
2. K. S. Novoselov, A. Mishchenko, A. Carvalho, 2D materials and van der Waals heterostructures. *Science* **353**, 9439 (2016).
3. B. Huang, G. Clark, E. Navarro-Moratalla, D. R. Klein, R. Cheng, K. L. Seyler, D. Zhong, E. Schmidgall, M. A. McGuire, D. H. Cobden, W. Yao, D. Xiao, P. Jarillo-Herrero, X. Xu, Layer-dependent ferromagnetism in a van der Waals crystal down to the monolayer limit. *Nature* **546**, 270 (2017).
4. J. Zak, E. R. Moog, C. Liu, S. D. Bader, Universal approach to magneto-optics. *J. Magn. Magn. Mater.* **89**, 107 (1990).
5. D. Zhong, Kyle L. Seyler, X. Linpeng, R. Cheng, N. Sivadas, B. Huang, E. Schmidgall, T. Taniguchi, K. Watanabe, M. A. McGuire, W. Yao, D. Xiao, Kai-Mei C. Fu, X. D. Xu, Van der Waals engineering of ferromagnetic semiconductor heterostructures for spin and valleytronics. *Sci. Adv.* **3**, e1603113 (2017).
6. M. Buscema, J. O. Island, D. J. Groenendijk, S. I. Blanter, G. A. Steele, H. S. J. van der Zant, A. Castellanos-Gomez, Photocurrent generation with two-dimensional van der Waals semiconductors, *Chem. Soc. Rev.* **44**, 3691 (2015).
7. B. Huang, G. Clark, D. R. Klein, D. MacNeill, E. Navarro-Moratalla, K. L. Seyler, N. Wilson, M. A. McGuire, D. H. Cobden, D. Xiao, W. Yao, P. Jarillo-Herreo, X. D. Xu, Electrical control of 2D magnetism in bilayer CrI₃. *Nat. Nano.* **13**, 544 (2018).
8. S. Jiang, L. Li, Z. Wang, K. F. Mak, J. Shan, Controlling magnetism in 2D CrI₃ by electrostatic doping. *Nat. Nano.* **13**, 549 (2018).
9. M. A. McGuire, H. Dixit, V. R. Cooper, B. C. Sales, Coupling of crystal structure and magnetism in the layered, ferromagnetic insulator CrI₃. *Chem. Mater.* **27**, 612 (2015).
10. A. Leon, J. W. González, J. Mejía, F. Lima, E. S. Morell, Strain-induced phase

transition in CrI₃ bilayers. Arxiv, 1911.09734.

11. C. Gong, L. Li, Z. Li, H. Ji, A. Stern, Y. Xia, T. Cao, W. Bao, C. Wang, Y. Wang, Z. Q. Qiu, R. J. Cava, S. G. Louie, J. Xia, X. Zhang, Discovery of intrinsic ferromagnetism in two-dimensional van der Waals crystals. *Nature* **546**, 265 (2017).
12. K. Wang, T. Hu, F. Jia, G. Zhao, Y. Liu, I. V. Solovyev, A. P. Pyatakov, A. K. Zvezdin, W. Ren, Magnetic and electronic properties of Cr₂Ge₂Te₆ monolayer by strain and electric-field engineering. *Appl. Phys. Lett.* **114**, 092405 (2019).
13. K. S. Burch, D. Mandrus, J.-G. Park, Magnetism in two-dimensional van der Waals materials. *Nature* **563**, 47 (2018).
14. N. Sivadas, S. Okamoto, X. D. Xu, C. J. Fennie, D. Xiao, Stacking-dependent magnetism in bilayer CrI₃. *Nano Lett.* **18**, 7658 (2018).
15. T. Song, Z. Fei, M. Yankowitz, Z. Lin, Q. Jiang, K. Hwangbo, Q. Zhang, B. Sun, T. Taniguchi, K. Watanabe, M. A. McGuire, D. Graf, T. Cao, J. H. Chu, D. H. Cobden, C. R. Dean, D. Xiao, X. Xu, Switching 2D magnetic states via pressure tuning of layer stacking. *Nat. Mater.* **18**, 1298 (2019).
16. T. Li, S. Jiang, N. Sivadas, Z. Wang, Y. Xu, D. Weber, J. E. Goldberger, K. Watanabe, T. Taniguchi, C. J. Fennie, K. F. Mak, J. Shan, Pressure-controlled interlayer magnetism in atomically thin CrI₃. *Nat. Mater.* **18**, 1303 (2019).
17. P. Jiang, C. Wang, D. Chen, Z. Zhong, Z. Yuan, Z.-Y. Lu, W. Ji, Stacking tunable interlayer magnetism in bilayer CrI₃. *Phys. Rev. B* **99**, 144401 (2019).
18. W. Chen, Z. Sun, Z. Wang, L. Gu, X. Xu, S. Wu, C. Gao, Direct observation of van der Waals stacking-dependent interlayer magnetism. *Science* **366**, 983 (2019).
19. J.-U. Lee, S. Lee, J. H. Ryoo, S. Kang, T. Y. Kim, P. Kim, C.-H. Park, J.-G. Park, H. Cheong, Ising-type magnetic ordering in atomically thin FePS₃. *Nano. Lett.* **16**, 7433 (2016).
20. M. Bonilla, S. Kolekar, Y. Ma, H. C. Diaz, V. Kalappattil, R. Das, T. Eggers, H. R. Gutierrez, M.-H. Phan, M. Batzill, Strong room-temperature ferromagnetism in VSe₂ monolayers on van der Waals substrates. *Nat. Nano.* **13**, 289 (2018).
21. D. J. O'Hara, T. Zhu, A. H. Trout, A. S. Ahmed, Y. K. Luo, C. H. Lee, M. R. Brenner, S. Rajan, J. A. Gupta, D. W. McComb, R. K. Kawakami, Room temperature intrinsic ferromagnetism in epitaxial manganese selenide films in the monolayer limit. *Nano. Lett.* **18**, 3125 (2018).
22. W. Zhang, L. Zhang, P. K. J. Wong, J. Yuan, G. Vinai, P. Torelli, G. van der Lann, Y. P. Feng, A. T. S. Wee, Magnetic transition in monolayer VSe₂ via interface

- hybridization. ACS Nano. **13**, 8997 (2019).
23. J. Li, Y. Li, S. Du, Z. Wang, B.-L. Gu, S.-C. Zhang, K. He, W.-H. Duan, Y. Xu, Intrinsic magnetic topological insulators in van der Waals layered MnBi_2Te_4 -family materials. Sci. Adv. **5**, eaaw5685 (2019).
 24. M. M. Otrokov, I. P. Rusinov, M. Blanco-Rey, M. Hoffmann, A. Yu. Vyazovskaya, S.V. Ereemeev, A. Ernst, P. M. Echenique, A. Arnau, E. V. Chulkov, Unique thickness-dependent properties of the van der Waals interlayer antiferromagnet MnBi_2Te_4 films. Phys. Rev. Lett. **122**, 107202 (2019).
 25. J. Li, C. Wang, Z. Zhang, B. L. Gu, W. H. Duan, Y. Xu, Magnetically controllable topological quantum phase transitions in the antiferromagnetic topological insulator MnBi_2Te_4 . Phys. Rev. B **100**, 121103 (2019).
 26. D. Zhang, M. Shi, T. Zhu, D. Xing, H.-J. Zhang, J. Wang, Topological axion states in the magnetic insulator MnBi_2Te_4 with the quantized magnetoelectric effect. Phys. Rev. Lett. **122**, 206401 (2019).
 27. Y. Gong, J. Guo, J. Li, K. Zhu, M. Liao, X. Liu, Q. Zhang, L. Gu, L. Tang, X. Feng, D. Zhang, W. Li, C. L. Song, L. L. Wang, P. Yu, X. Chen, Y. Y. Wang, H. Yao, W. H. Duan, Y. Xu, S.-C. Zhang, X. C. Ma, Q.-K. Xue, K. He, Experimental realization of an intrinsic magnetic topological insulator. Chin. Phys. Lett. **36**, 7 (2019).
 28. C. Liu, Y. Wang, H. Li, Y. Wu, Y. Li, J. Li, K. He, Y. Xu, J. Zhang, Y. Wang, Quantum phase transition from axion insulator to Chern insulator in MnBi_2Te_4 . Nat. Mater. **1** (2020)
 29. Y. Deng, Y. Yu, M. Z. Shi, Z. Guo, Z. Xu, J. Wang, X. H. Chen, Y. Zhang, Magnetic-field-induced quantized anomalous Hall effect in intrinsic magnetic topological insulator MnBi_2Te_4 . Science **367**, 895 (2020).
 30. R. C. Vidal, H. Bentmann, T. R. F. Peixoto, A. Zeugner, S. Moser, C.-H. Min, S. Schatz, K. Kißner, M. Unzelmann, C. I. Fornari, H. B. Vasili, M. Valvidares, K. Sakamoto, D. Mondal, J. Fujii, I. Vobornik, S. Jung, C. Cacho, T. K. Kim, R. J. Koch, C. Jozwiak, A. Bostwick, J. D. Denlinger, E. Rotenberg, J. Buck, M. Hoesch, F. Diekmann, S. Rohlf, M. Kallane, K. Rossnagel, M. M. Otrokov, E. V. Chulkov, M. Ruck, A. Isaeva, F. Reinert, Surface states and Rashba-type spin polarization in antiferromagnetic MnBi_2Te_4 (0001). Phys. Rev. B **100**, 121104 (2019).
 31. A. Zeugner, F. Nietschke, A. U. B. Wolter, S. Gaß, R. C. Vidal, T. R. F. Peixoto, D. Pohl, C. Damm, A. Lubk, R. Hentrich, S. K. Moser, C. Fornari, C. H. Min, S. Schatz, K. Kißner, M. Unzelmann, M. Kaiser, F. Scaravaggi, B. Rellinghaus, K. Nielsch, C. Hess, B. Buchner, F. Reinert, H. Bentmann, O. Oeckler, T. Doert, M. Ruck, A.

- Isaeva, Chemical aspects of the candidate antiferromagnetic topological insulator MnBi_2Te_4 . *Chem. Mater.* **31**, 2795 (2019).
32. Y. J. Hao, P. Liu, Y. Feng, X. M. Ma, E. F. Schwier, M. Arita, S. Kumar, C. W. Hu, R. Lu, M. Zeng, Y. Wang, Z. Y. Hao, H. Y. Sun, K. Zhang, J. W. Mei, N. Ni, L. Wu, K. Shimada, C. Y. Chen, Q. H. Liu, C. Liu, Gapless surface Dirac cone in antiferromagnetic topological insulator MnBi_2Te_4 . *Phys. Rev. X* **9**, 041038 (2019).
 33. J. Ge, Y. Liu, J. Li, H. Li, T. Luo, Y. Wu, Y. Xu, J. Wang, High- Chern-number and high-temperature quantum Hall effect without Landau levels. *Arxiv*, 1907.09947.
 34. H. X. Fu, C. X. Liu, B. H. Yan, Exchange bias and quantum anomalous Hall effect in the $\text{MnBi}_2\text{Te}_4\text{-CrI}_3$ heterostructure. *Arxiv*, 1908.04322.
 35. M. Z. Hasan, C. L. Kane, Colloquium: Topological insulators. *Rev. Mod. Phys.* **82**, 3045 (2010).
 36. X.-L. Qi, S.-C. Zhang, Topological insulators and superconductors. *Rev. Mod. Phys.* **83**, 1057 (2011).
 37. X.-L. Qi, T. L. Hughes, and S.-C. Zhang, Topological field theory of time-reversal invariant insulators. *Phys. Rev. B* **78**, 195424 (2008).
 38. J. E. Moore, The birth of topological insulators. *Nature* **464**, 194 (2010).
 39. R. S. K. Mong, A. M. Essin, J. E. Moore, Antiferromagnetic topological insulators. *Phys. Rev. B* **81**, 245209 (2010).
 40. G. Kresse, J. Furthmüller, Efficient iterative schemes for ab initio total-energy calculations using a plane-wave basis set. *Phys. Rev. B* **54**, 11169 (1996).
 41. J. P. Perdew, K. Burke, M. Ernzerhof, Generalized gradient approximation made simple. *Phys. Rev. Lett.* **77**, 3865 (1996).
 42. A. D. Becke, E. R. Johnson, A simple effective potential for exchange. *J. Chem. Phys.* **124**, 221101 (2006).
 43. S. Grimme, J. Antony, S. Ehrlich, H. Krieg, A consistent and accurate ab initio parametrization of density functional dispersion correction (DFT-D) for the 94 elements. *J. Chem. Phys.* **132**, 154104 (2010).
 44. Q. Wu, S. Zhang, H.-F. Song, M. Troyer, A. A. Soluyanov, WannierTools: An open-source software package for novel topological materials. *Comput. Phys. Commun.* **224**, 405 (2018).
 45. John B. Goodenough, Magnetism and chemical bond. Interscience Publ, **Vol.1** (1963).

46. E. Koch, "Exchange mechanisms." *Correlated electrons: from models to materials*. **2**, 1 (2012).
47. Y. H. Matsuda, Z. W. Ouyang, H. Nojiri, X-Ray magnetic circular dichroism of a valence of fluctuating state in Eu at high magnetic fields. *Phys. Rev. Lett.* **103**, 046402 (2019).
48. X. Wan, A. M. Turner, A. Vishwanath, Topological semimetal and Fermi-arc surface states in the electronic structures of pyrochlore iridates. *Phys. Rev. B* **83**, 205101 (2011).
49. F. D. M. Haldane, Model for a quantum Hall effect without Landau levels: Condensed matter realization of the "parity anomaly". *Phys. Rev. Lett.* **61**, 2015 (1988).
50. R. Yu, W. Zhang, H. Zhang, S.-C. Zhang, X. Dai, Z. Fang, Quantized Anomalous Hall Effect in Magnetic Topological Insulators. *Science* **329**, 61 (2010).
51. A. A. Burkov, L. Balents, Weyl semimetal in a topological insulator multilayer. *Phys. Rev. Lett.* **107**, 127205 (2011).
52. G. Xu, H. Wen, Z. Wang, X. Dai, Z. Fang, Chern semimetal and the quantized anomalous Hall effect in HgCr_2Se_4 . *Phys. Rev. Lett.* **107**, 186806 (2011).
53. A. A. Soluyanov, D. Gresch, Z. Wang, Q. S. Wu, M. Troyer, X. Dai, B. A. Bernevig, Type-II Weyl Semimetals. *Nature* **527**, 495 (2015).
54. C.-Z. Chang, J. Zhang, X. Feng, J. Shen, Z. Zhang, M. Guo, K. Li, Y. Ou, P. Wei, L.-L. Wang, Z.-Q. Ji, Y. Feng, S. Ji, X. Chen, J. Jia, X. Dai, Z. Fang, S.-C. Zhang, K. He, Y. Wang, L. Lu, X.-C. Ma, Q.-K. Xue, Experimental Observation of the Quantum Anomalous Hall Effect in a Magnetic Topological Insulator. *Science* **340**, 167(2013).
55. C.-Z. Chang, W. Zhao, D. Y. Kim, H. Zhang, B. A. Assaf, D. Heiman, S.-C. Zhang, C. Liu, M. H. W. Chan, J. S. Moodera, High-precision realization of robust quantum anomalous Hall state in a hard ferromagnetic topological insulator. *Nat. Mater.* **14**, 473 (2015).
56. H. Zhang, C.-X. Liu, X.-L. Qi, X. Dai, Z. Fang, S.-C. Zhang, Topological insulators in Bi_2Se_3 , Bi_2Te_3 and Sb_2Te_3 with a single Dirac cone on the surface. *Nat. Phys.* **5**, 438 (2009).

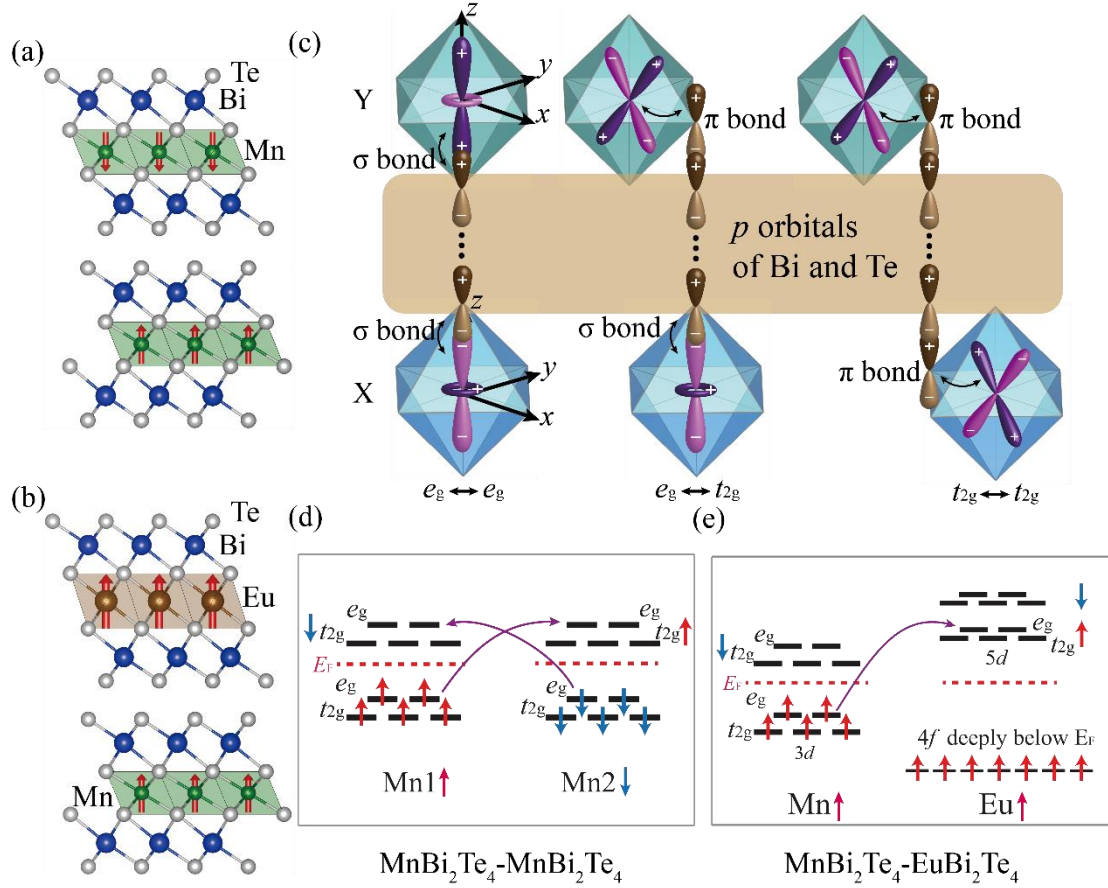


Figure 1. (a, b) Schematic lattice structures (side view) of (a) a MnBi₂Te₄-MnBi₂Te₄ bilayer and (b) a MnBi₂Te₄-EuBi₂Te₄ bilayer. The red arrows indicate the spin directions. (c) Schematic drawings of three hopping channels supporting the superexchange interlayer magnetic coupling: e_g - p - e_g (left), e_g - p - t_{2g} (middle) and t_{2g} - p - t_{2g} (right). X and Y denote two magnetic atoms in XBi₂Te₃-YBi₂Te₃. (d, e) Schematic drawings of the energy levels of magnetic atoms and the hopping channels between them in MnBi₂Te₃-MnBi₂Te₄ (d) and in MnBi₂Te₃-EuBi₂Te₄ (e).

TABLE 1: The magnetic ground states and the interlayer exchange energies (E_{ex}) which is the energy difference between the A-type AFM state and FM state of XBi_2Te_3 - YBi_2Te_3 bilayers (X, Y represents Ni, Mn, V, or Eu).

$E_{\text{ex}}/(\text{meV})$	X				
	Ni($3d^8$)	Mn($3d^5$)	V($3d^3$)	Eu($4f^7+5d^0$)	
Y	Ni($3d^8$)	AFM -16.5	AFM -4.6	FM +3.5	FM +1.1
	Mn($3d^5$)	AFM -4.6	AFM -1.3	FM +1.2	FM +0.6
	V($3d^3$)	FM +3.5	FM +1.2	AFM -0.5	AFM -0.2
	Eu($4f^7+5d^0$)	FM +1.1	FM +0.6	AFM -0.2	AFM -0.1

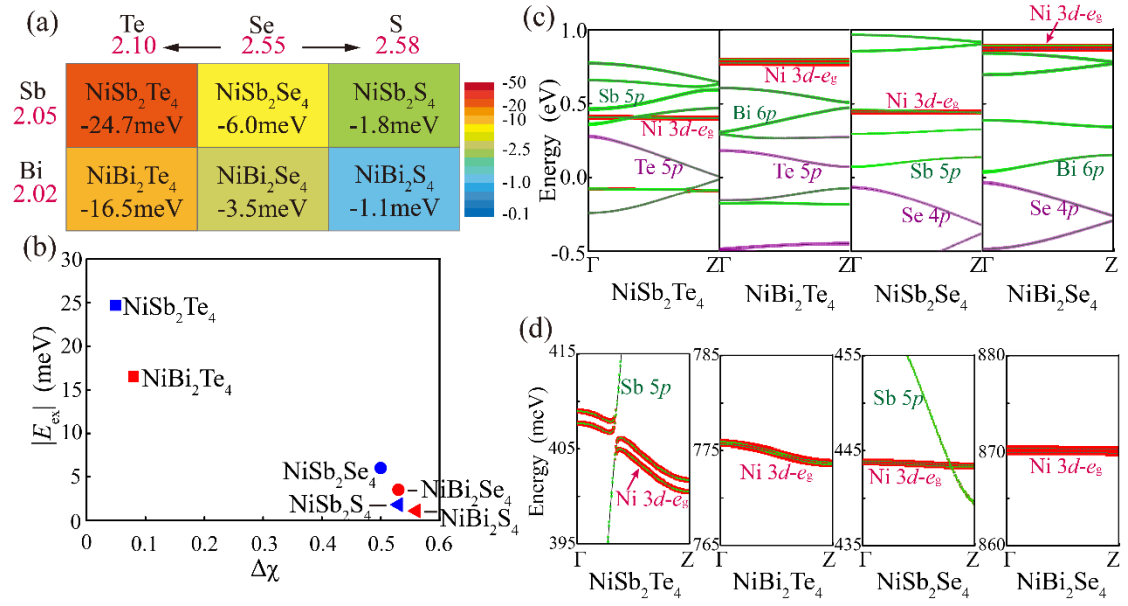


Figure 2. (a) Table of the interlayer magnetic coupling (IMC) strength ($|E_{\text{ex}}|$) of six compounds of $\text{Ni(V)}_2(\text{VI})_4$, in which (V) = Bi, Sb; (VI) = Te, Se, S. Electronegativity (χ) of each element is noted below as red digits. (b) Dependence of $|E_{\text{ex}}|$ on the electronegativity difference ($\Delta\chi$) between the anions (VI) and nonmagnetic cations (V) of six $\text{Ni(V)}_2(\text{VI})_4$. (c) Dispersions of element-projected bands along $\Gamma - Z$ directions of NiSb_2Te_4 , NiBi_2Te_4 , NiSb_2Se_4 , and NiBi_2Se_4 . Red curves denote the Ni 3d- e_g bands. Green and purple curves denote the p bands of (V) and (VI), respectively. (d) Zoom-in figures near the Ni 3d- e_g bands in the four materials.

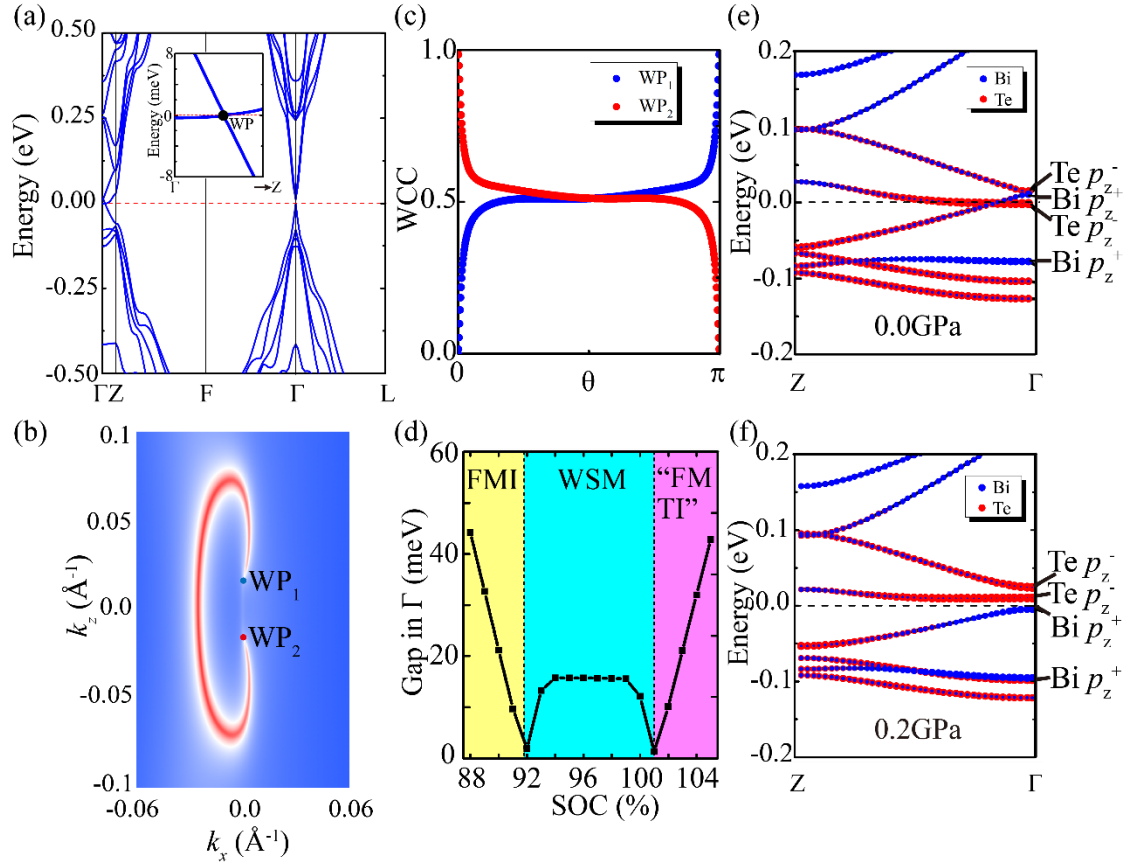


Figure 3. Band structures and topological features of bulk $\text{MnBi}_2\text{Te}_4\text{-EuBi}_2\text{Te}_4$. (a) Band structures of bulk $\text{MnBi}_2\text{Te}_4\text{-EuBi}_2\text{Te}_4$ superlattice. The inset shows a weakly dispersed band along the Γ -Z direction, implying the type-I WSM nature. (b) Surface states on the (110) plane at the energy of the two Weyl points (WP_1 and WP_2). (c) The motions of the sum of Wannier charge centers on a sphere surrounding each of two Weyl points in the momentum space. (d) Band gap at Γ as a function of the strength of spin-orbit coupling. The three areas of different colors denote different topological phases. (e, f) Element-projected bandstructures of Bi p_z and Te p_z orbitals along $Z - \Gamma$ direction under (e) zero pressure and (f) external 0.2GPa hydrostatic pressure, respectively. “+” and “-” signs denote even and odd parities, respectively.

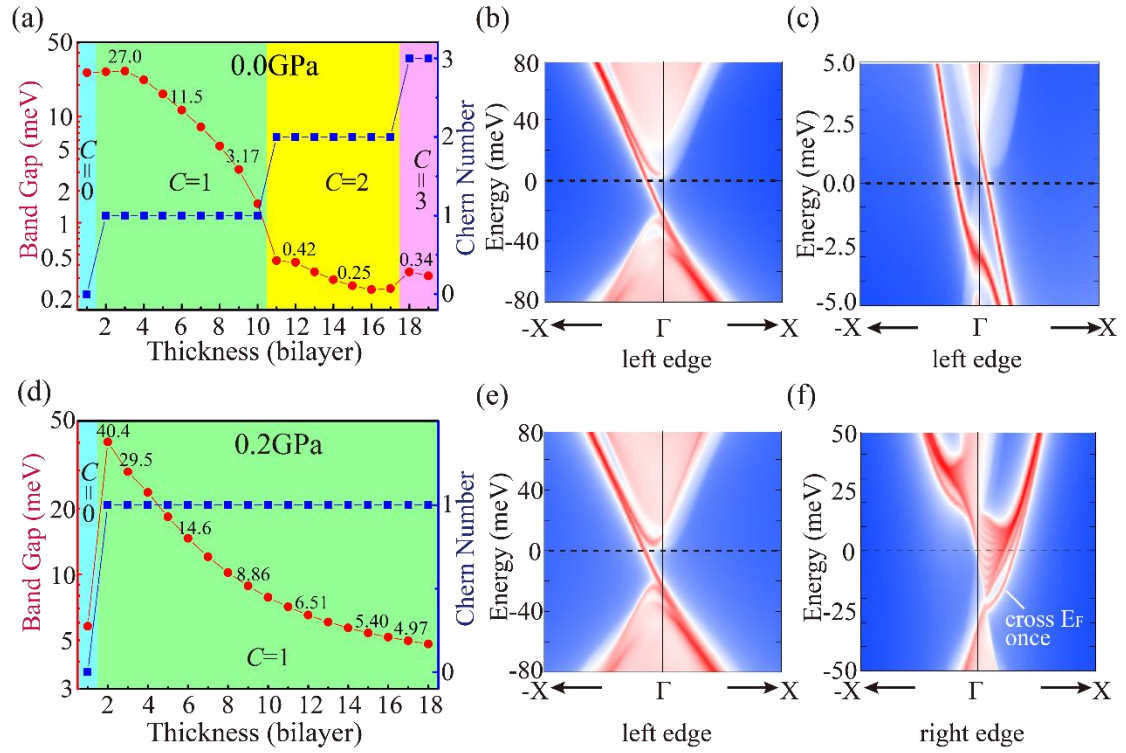


Figure 4. Topological features of MnBi₂Te₄-EuBi₂Te₄ superlattice thin films. (a, d) The band gap size at Γ point (red) and the Chern number (blue) of MnBi₂Te₄-EuBi₂Te₄ thin film with increasing film thickness under hydrostatic pressure of (a) zero and (d) 0.2 GPa. The areas of different colors represent the phases with different Chern numbers. (b, c) Edge states of (b) a film of 3 MnBi₂Te₄-EuBi₂Te₄ bilayers and (c) a film of 12 MnBi₂Te₄-EuBi₂Te₄ bilayers without external pressure, which show one and two chiral edge states, respectively. (c, e) Edge states of (e) a film of 3 MnBi₂Te₄-EuBi₂Te₄ bilayers and (f) a film of 12 MnBi₂Te₄-EuBi₂Te₄ bilayers under 0.2 GPa, both of which exhibit one chiral edge state.